JOURNAL OF SPACECRAFT AND ROCKETS
Vol. 35, No. 5, September–October 1998

Calibration of Accelerometers for the Measurement of Microvibrations

Julián Santiago-Prowald,* Francisco J. Reina-Barragán,† and Ángel Sanz-Andrés‡
Universidad Politécnica de Madrid, Ciudad Universitaria, 28040 Madrid, Spain
and
Luis Muñoz-Sevilla§
Construcciones Aeronáuticas S.A., 28022 Madrid, Spain

The accelerometers used for the measurement of microvibrations or microgravity applications, such as active control of space structures, attitude control, scientific payloads, or even on-Earth testing of structures at very low-excitation levels, require a dedicated calibration procedure that includes the gravitational effects. Otherwise, on-Earth calibrations can be inaccurate due to the collateral projection of the local gravity onto the sensitive axis. An on-Earth calibration technique for the 10^{-7}–10^{-2}-g amplitude range and 0–100-Hz frequency range is described. Special attention has been given to the modeling of gravitational effects on the response of the calibration device and the accelerometer itself. The sensitivity and resolution tests performed on piezoelectric accelerometers show the accuracy and the potential of this technique. Typical scale factor uncertainty, which has been carefully analyzed, is of the order of 2% at acceleration levels of 10^{-5} g.

Nomenclature

$\boldsymbol{A}$	= net acceleration vector projected on the pendulum reference, m/s^2
A	= dimensionless pendulum parameter, related to the characteristic frequency x_1; Eq. (3)
B	= dimensionless pendulum parameter, related to the excitation amplitude; Eq. (3)
C	= dimensionless pendulum parameter, related to the frequency x_2, $L_a\Omega_0^2/g$
C_i	= influence coefficient of the magnitude i in the global uncertainty
$\boldsymbol{e}$	= sensitive axis of the accelerometer
$\boldsymbol{g}$	= local gravity acceleration vector, m/s^2
g_0	= reference acceleration of gravity, 9.80665 m/s^2
H_{os}	= sensitivity of the optical sensor, V/m
I	= moment of inertia of the calibration pendulum excluding the contribution of the excitation mass, kg · m^2
L	= rotation radius, m
L_{os}	= optical radius of measurement, m
L_1	= length of the pendulum beam, m
M	= mass of the pendulum excluding the excitation mass, kg
m	= excitation mass, kg
SF	= scale factor or sensitivity of the accelerometer, V/g or pC/g
u	= displacement of the excitation mass referenced to the pendulum, m
u_i	= uncertainty of the magnitude i
$\boldsymbol{u}_r$, $\boldsymbol{u}_\theta$	= unit reference vectors bounded to the calibration pendulum
V	= output voltage, V
x	= dimensionless excitation frequency; Eq. (3)
$\|x\|$	= amplitude of magnitude x
x_1	= dimensionless zero-oscillation-amplitude frequency, $1/\sqrt{A}$
x_2	= dimensionless zero-acceleration-amplitude frequency, $1/\sqrt{C}$
γ	= nondimensional effective damping coefficient
Δ	= damped period of oscillation in damping test, s
δ	= centering parameter with respect to the pendulum centerline, m
$\delta\alpha$, $\delta\beta$	= misalignment angles of the sensitive axis with respect to the pendulum axes
ε	= balance error angle, rad
θ	= oscillation angle of the pendulum with respect to the local vertical, rad
λ	= transverse sensitivity coefficient
Ω_p	= contribution of parasitic stiffness to nondamped eigenfrequency, Hz
Ω_0	= nondamped eigenfrequency of the rigid-body rotation without parasitic stiffness
Ω_0'	= nondamped eigenfrequency of the rigid-body rotation with parasitic stiffness, Hz
Ω_1	= damped eigenfrequency of the rigid-body rotation with parasitic stiffness, Hz
ω	= frequency of the excited movement, Hz

Subscripts

a	= accelerometer
e	= excitation
M	= pendulum excluding excitation mass
m	= excitation mass
os	= optical sensor
r, θ	= radial and azimuthal directions
$0, \infty$	= zero and high frequency, respectively

Received Jan. 26, 1998; revision received June 1, 1998; accepted for publication June 10, 1998.

*Engineer, Instituto Universitario "Ignacio Da Riva," Laboratorio de Aerodinámica, Escuela Técnica Superior de Ingenieros Aeronáuticos.
†Research Scientist, Instituto Universitario "Ignacio Da Riva," Laboratorio de Aerodinámica, Escuela Técnica Superior de Ingenieros Aeronáuticos.
‡Associate Professor, Instituto Universitario "Ignacio Da Riva," Laboratorio de Aerodinámica, Escuela Técnica Superior de Ingenieros Aeronáuticos. Member AIAA.
§Engineer, Space Division, Department of Integration and Testing, Avda. de Aragón, 404.

Introduction

THE accelerometers used for microgravity or microvibration applications must be calibrated taking into account the effect of the different gravitational environments, i.e., the 1-g on-Earth environment compared to the microgravity orbital environment. Typical applications that require an on-Earth calibration with the purpose of characterizing the behavior of the accelerometers in the low-level range are as follows:

1) The prediction of the response of space structures requires modeling and on-Earth testing. When considering active control of

the structures and its coupling with attitude control, the effect of the different gravitational environments must be introduced in the models.[1] Intensive testing is usually necessary for two reasons: the determination of parameters and the validation of the models. For these tests, particularly in closed-loop operation, highly reliable accelerometers and a careful analysis of the measurements are needed.

2) Scientific payloads usually require the measurement or knowledge of the microgravity perturbations to correlate them with the experimental results. This is extremely important in the particular case of experiments involving fluids. The residual gravity (quasisteady perturbation) is known to modify the equilibrium shapes of slender liquid bridges.[2] This fact has led to their use as highly sensitive accelerometers. Time-dependent perturbations, known as g jitter, also have an influence on fluid configurations, especially in the presence of temperature and concentration gradients.[3,4] Consequently, reference accelerometers are needed, and their on-Earth calibration must account for the effect of the local gravity. In the case of quasisteady measurements, the bias and the sensitivity of Q-flex accelerometers obtained from on-Earth calibration cannot be directly extrapolated to the in-orbit operation.[5] Hence, gravity-dependent response models are unavoidable if in-orbit calibration cannot be afforded.[6]

3) The design of complex space systems includes specifications of vibration transmission from components to subsystems and vice versa. Such specifications are required for the international space station (ISS). Vibration requirements have been imposed on ISS systems and payloads; acceptable levels are given by the Naumann curve,[7] which specifies a 1-μg rms vibration level in the quasisteady range. Ground tests are thus necessary for the determination of the vibration level transmitted. The European Space Agency's ARTEMIS spacecraft also has strong requirements on the vibration transmission to guarantee the pointing accuracy of the SILEX optical payload.[8]

Calibration devices such as electromechanical shaking tables lack accuracy when excited at very low amplitudes. One reason is the undetermined projection of the environmental gravity, which can become of the same order of magnitude as the excited acceleration. As a general rule, an acceleration amplitude of 1 μg can be confused with a microradian oscillatory misalignment. Hence, the development of specific devices and techniques is needed for the microgravity range.

An on-Earth calibration technique for accelerometers devoted to the measurement of microvibrations using standard equipment is proposed. Although the procedures do not depend on the accelerometer type, the models are specifically adapted to piezoelectric accelerometers. Other applications of the technique can be found in previous works.[6] In the following, the concept of the calibration setup, the response models, and the tests performed on the engineering model are described. Uncertainties are carefully analyzed to characterize the quality of the measurements. The technique is applied to two commercial accelerometers at very low acceleration levels, down to 10^{-7} g, showing successful results and, most important, the potential of high-quality calibration for microvibration applications.

Calibration Technique and Models of the Response

The calibration technique is based on the generation of microaccelerations by means of a specially developed facility, the calibration pendulum. This instrument has been designed and tested for generating reference accelerations in the range 10^{-7}–10^{-2} g between 0 and 100 Hz. The calibration procedure is indirect; reference data must be generated to determine the input to the sensor and the scale factor. However, due to the pendulum oscillations, not only are reference accelerations generated, but also a collateral projection of the local gravity acceleration on the sensitive axis appears. When dealing with microaccelerations, this effect must be modeled to avoid errors in the measurements of the same order of magnitude as the measurement itself.

The calibration concept is shown in Fig. 1 and follows that presented in Ref. 6. The motion of the pendulum is produced by the displacement of the excitation mass. The reference signal is obtained by the measurement of the pendulum excited oscillations by means of a high-resolution optical displacement sensor (Keyence

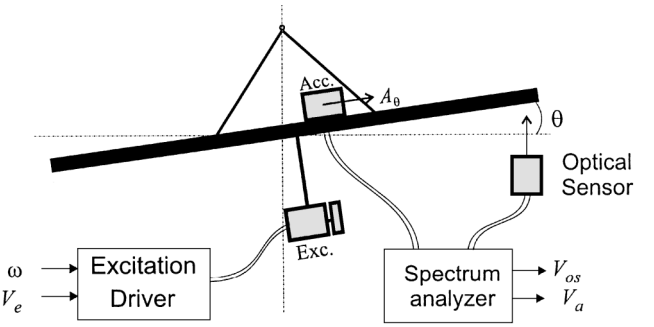

Fig. 1 Calibration concept; the tangential acceleration A_θ is proportional to the oscillation amplitude $|\theta|$.

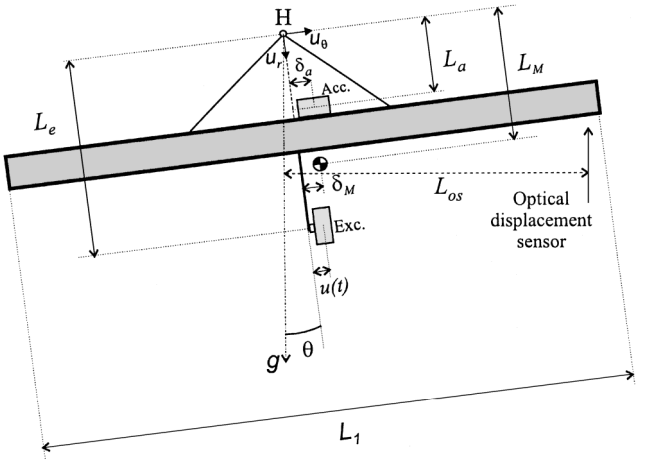

Fig. 2 Geometry of the pendulum.

PA-1810). This allows the determination of the acceleration and the local gravity, both projected onto the sensitive axis. By comparing the net acceleration to the accelerometer output, the scale factor is obtained, in either volts per acceleration of gravity (9.80665 m/s^2) or picocoulomb per acceleration of gravity, depending on the accelerometer type. The measured scale factor, defined as the amplitude ratio of the accelerometer output $|V_a|$ and the net acceleration in the tangential direction of the motion $|A_\theta|$, is given by

$$\mathrm{SF}(\omega) = |V_a|/|A_\theta| \tag{1}$$

This scale factor is affected by the uncertainties that arise from the determination of the parameters and the measurements themselves.

Calibration Pendulum Model

A detailed model of the pendulum and the accelerometer response is required to design for a specific measurement range and to define the procedures. The geometric parameters of the pendulum, whose model is given in the Appendix, are shown in Fig. 2. It consists of a beam of length L_1 hanging horizontally from a hinge point H with the center of mass at a distance L_M. The only rigid-solid degree of freedom is the rotation of the beam, θ, around the point H. The accelerometer is placed on the beam with the radius of rotation L_a and its sensitive axis oriented tangentially. Also attached to the beam, the excitation system is located at a distance L_e. The parameters δ_m will be used for balancing the pendulum and δ_a for controlling measurement errors. The values of these parameters, the excitation mass m, and the mass of the rest of the system M will be obtained from the design process.

The differential equation (A3) in the Appendix represents the linear model of the pendulum. The oscillation amplitude response is

$$|\theta| = \frac{B|Ax^2 - 1|}{\sqrt{(1 - x^2)^2 + 4\gamma^2 x^2}} \tag{2}$$

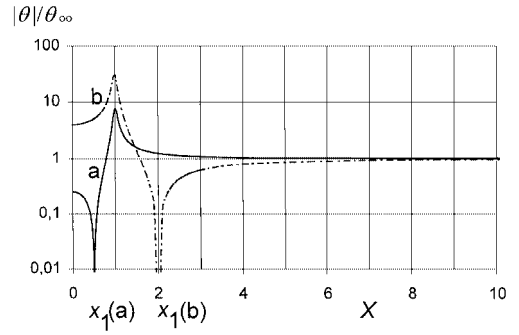

Fig. 3 Effect of the parameter A in the amplitude response of the pendulum as a function of $x = \omega/\Omega_0'$. A(a) = 4.0, A(b) = 0.25. B = 0.002 and γ = 0.05 for both.

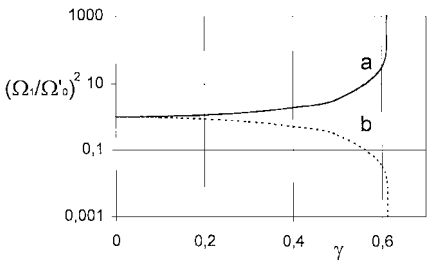

Fig. 4 Effect of the damping parameter γ on Ω_1; A(a) = 4.0, A(b) = 0.25.

where

$$x = \frac{\omega}{\Omega_0'}, \qquad A = \frac{L_e}{g}\Omega_0'^2, \qquad B = \frac{m|u|g}{\left[I + m\left(L_e^2 + \delta_m^2\right)\right]\Omega_0'^2} \tag{3}$$

and γ is a nondimensional global damping coefficient that includes friction as the main effect. Figure 3 shows $|\theta|$ as a function of x for $A = 0.25$ and 4. The phase response experiences 180-deg jumps across the resonance frequency $x = 1$ and $x = x_1 = 1/\sqrt{A}$. The effective nondamped eigenfrequency Ω_0' consists of two contributions: one deduced directly from the dynamic model of the Appendix and the other resulting from a parasitic stiffness arising from the connecting wires. Thus, we can write

$$\Omega_0'^2 = \Omega_p^2 + \Omega_0^2 = \Omega_p^2 + \frac{(ML_M + mL_e)g}{I + m\left(L_e^2 + \delta_m^2\right)} \tag{4}$$

Consequently, the system can be described with the three nondimensional parameters A, B, and γ. Their determination and use for the pendulum design process is supported by the following characteristic values: 1) amplitude for high frequencies ($\omega \to \infty$), $|\theta| = \theta_\infty = AB$; 2) amplitude for small frequencies ($\omega \to 0$), $|\theta| = \theta_0 = B$; and 3) frequency for zero amplitude ($|\theta| = 0$), $x = x_1 = 1/\sqrt{A}$.

It can be observed that two different characteristic frequency-response curves can be obtained, depending on the parameter A (Fig. 3). For $A > 1$, which means $g/L_e > \Omega_0'^2$, the frequency of zero amplitude lies below the eigenfrequency. The two curves shown belong to $A < 1$ and $A > 1$. A singular case is $A = 1$, very difficult to reproduce experimentally, in which the amplitude response is flat.

The damping coefficient avoids having the infinite amplitude at resonance and changes slightly the frequency of maximum amplitude, but the parameters A and B do not depend on γ and, hence, the general shape of the amplitude response does not change significantly. Equation (A4) gives the frequency of maximum amplitude Ω_1. Depending on whether A is greater or less than unity, Ω_1 can be greater or less than the nondamped eigenfrequency, respectively (Fig. 4). The worst case would represent an infinite Ω_1 for high damping, which results from an extreme flattening of the amplitude response and the absence of a maximum-amplitude point. These results will be considered for the experimental determination of the actual pendulum parameters.

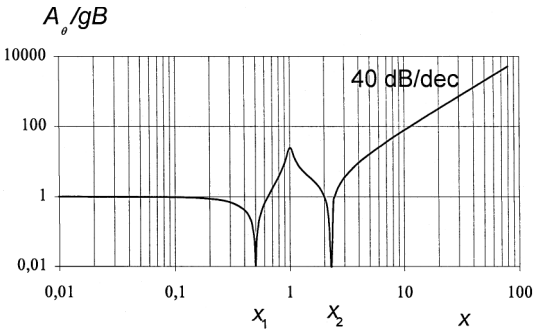

Fig. 5 Typical acceleration response on the pendulum for A = 4, B = 0.002, and γ = 0.05.

Accelerometer Model

The calibration of accelerometers on the pendulum is based on the precise determination of their response to the excited motion. This response is proportional to the net acceleration (defined as the combined effect of the acceleration and gravity fields on the accelerometer's seismic mass) projected on the sensitive axis. For this purpose, it is required to have a model for the functional dependence of the net acceleration on the oscillation amplitude $|\theta|$, the excitation frequency ω, and the local gravity g. In the following, the net acceleration model will be applied to piezoelectric transducers. The sensitive axis is assumed to be tangential to the direction of motion. (Misalignment will be considered only for the analysis of measurement errors.) Under these assumptions, it can be proven that only the rotation radius L_a, and not the centering parameter δ_a, appears in the expression for the net acceleration in the tangential direction, i.e.,

$$A_\theta = \left(g - L_a\omega^2\right)|\theta(\omega)| \sin \omega t \tag{5}$$

In this result, the linear distribution of the acceleration field acting on the seismic mass has been taken into account. Figure 5 is a typical acceleration response of the accelerometer on the pendulum using Eq. (5). Another zero-amplitude point appears at the frequency $x = x_2 = 1/\sqrt{C}$, where $C = L_a\Omega_0'^2/g$. For high frequencies, the acceleration is quadratic on x; in a log-log plot it approaches the straight line $\log(|A_\theta|/g) = \log(ABC) + 2\log x$, which has the slope 40 dB/decade. The acceleration phase experiences 180-deg jumps at $x = x_1$, 1, and x_2.

The parameter δ_a influences the radial acceleration and, hence, the transverse sensitivity and misalignment error. The normal-to-tangential ratio is given by

$$\frac{|A_r|}{|A_\theta|} = \frac{\delta_a\omega^2}{\left|g - L_a\omega^2\right|} \tag{6}$$

and will be used for the uncertainty analysis.

Pendulum: Design and Validation

The pendulum must be designed with the requirement of generating accelerations in the range of 10^{-7}–10^{-2} g. This requirement gives sufficient conditions for sizing the dimensionless parameters A and B. In a first approach, the damping coefficient can be set to zero. From A and B and other practical considerations, the dimensional parameters can be determined. Restrictions are imposed by the accuracy of the output measurements and by the optical resolution, which is 1 μm for the chosen sensor. Because the lowest acceleration level depends on the amplitude resolution of the available excitation device, only the upper acceleration level can be imposed. Notice that frequency and acceleration are not independent; the latter behaves as the square of the former at high frequencies (Fig. 5). This implies that high acceleration levels will be obtained at high frequencies and that the most critical design limit is the upper acceleration level. The two principal conditions are, thus, the optical resolution, with a safety factor, and the maximum acceleration

$$(L_1/2)|\theta| \geq 5\ \mu\text{m} \tag{7}$$

$$\frac{|A_\theta|}{g_0} = \left|\frac{L_a\omega^2}{g_0} - \frac{g}{g_0}\right||\theta| \leq 10^{-2} \tag{8}$$

Table 1 Design point of the calibration pendulum

Parameter	Unit	Estimated value	Variability
$u_{0\,\max}$	m	20×10^{-6}	$0\text{–}20 \times 10^{-6}$ [a]
L_1	m	1.000	± 0.1 [b]
L_a	m	0.022	± 0.002 [c]
L_M	m	0.100	± 0.05 [b]
L_e	m	0.175	± 0.01 [b]
m	kg	0.750	0.5–1.0 [b]
M	kg	2.000	± 0.5 [b]
Ω_0'	rad/s	8.2	5–12 [c]
A	——	1.2	0.5–5.0 [b]
B	——	1.1×10^{-5}	5×10^{-6}–5×10^{-5} [a]
γ	——	0	0.0–0.5 [b]

[a]Control parameter. [b]Design margin. [c]Uncertainty.

Hence, the maximum frequency that can be obtained for a given tangential acceleration depends on the minimization of the product $L_a|\theta|$. The minimum practical value for L_a is 1 cm in the present configuration, whereas the lowest oscillation amplitude $|\theta|$ is limited by the optical resolution. From Eq. (7), the higher L_1 is, the weaker the optical resolution requirement on the oscillation amplitude, and therefore, from Eq. (8), the maximum compatible frequency can be increased. With $L_1 = 1$ m (the highest practical value considered), the amplitude for maximum frequency is $|\theta(\omega_{\max})| = 10\ \mu$rad. Considering the high-frequency asymptotic value of the pendulum, this leads to $\theta_\infty = AB = 10\ \mu$rad. With AB fixed at high frequencies for the lowest measurable amplitude, B can be increased at lower frequencies using the excitation parameter $|u|$ to obtain higher oscillation amplitudes and reduce errors. With these requirements, a first approximation for the maximum frequency is $\omega_{\max} = \sqrt{[10^{-2}\, g_0/(\theta_\infty L_a)]} \approx 150$ Hz.

After applying the requirements to the nondimensional parameters, the dimensional parameters must be sized. This sizing is a delicate tradeoff process, depending on the characteristics of the equipment available. See Table 1 for our particular design point. Of remarkable difficulty is the estimate of the nondamped eigenfrequency. Our experience has shown that the parasitic stiffness introduces a factor of about 2 in the eigenfrequency, causing the coefficient A to jump above 1.

Another important effect of the length of the beam is the control of the bending eigenfrequencies because of their proportionality to $1/L_1^2$, thus imposing another limit to the maximum frequency. The pendulum beam has been made with an aluminum tube with the lowest eigenfrequency corresponding to the first bending mode with free-free boundaries.[9] Hence, $f_1(\text{Hz}) = 4.7^2\sqrt{(EI/M_b)}/(2\pi L_1^2) \approx 170$ Hz, higher than $\omega_{\max}$.

To determine the actual value of the parameters and validate the model of the pendulum, comparison with tests is required. The validation procedure proposed is based on the determination of parameters by experiments and the subsequent comparison of model and measured response. Note that, although the determination of the pendulum parameters is not essential to the calibration concept, it is needed for the pendulum control. The parameters that require determination are A, B, γ, and the nondamped eigenfrequency Ω_0'. A standard damping test, needed to determine Ω_0' and γ (and, hence, Ω_1 and A, assumed L_e and the local gravity known), will be described and applied. The exact determination of B is, however, extremely difficult and can be obtained only from an experimental amplitude response. Both tests are described in the following section. Procedures based on phase jumps have not been used because they require an extremely accurate frequency measurement and are subject to nonlinear effects.

Damping Test

The method used is the logarithmic decrement. Nonforced oscillations of the pendulum are recorded after a small displacement from its equilibrium. The expected time response is a typical damped oscillation of the form $\theta = C_1 \exp(-\gamma\Omega_0' t)\sin(\Omega_0'\sqrt{(1-\gamma^2)}t + C_2) + \varepsilon$. The constants depend on the initial conditions at the release. Taking the logarithm and subtracting the last expression evaluated at two different times t and $t' = t + n\Delta$, where n is an integer and $\Delta = 2\pi/[\Omega_0'\sqrt{(1-\gamma^2)}]$, we have

$$\ell n\,\theta - \ell n\,\theta' = \frac{2\pi n\gamma}{\sqrt{1-\gamma^2}} \tag{9}$$

Both γ and Ω_0' are then determined. As a consequence, assuming L_e known from the geometry, A can be calculated using Eq. (3).

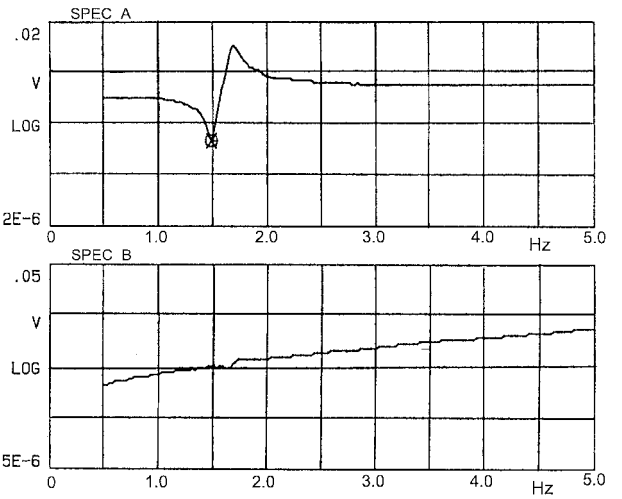

Fig. 6 Measured amplitudes of oscillation (spectrum A) and ISOS-HEAR acceleration output (spectrum B) vs excitation frequency with $|u| = |u|_{\max}/4 \approx 5\ \mu$m, $L_a = 94$ mm, pointer (⊗) at 1.475 Hz, $V_{os} = 1.01E-4$ V, $V_a = 5.19E-4$ V, and frequency resolution $\Delta f = 0.025$ Hz.

Amplitude-Response Test

A frequency sweep of the excitation at fixed $|u|$ is applied in the range of interest, and the outputs of the optical sensor and the accelerometer are recorded (Fig. 6). The measurement of the pendulum oscillation amplitude as a function of frequency allows the determination of $\theta_\infty = AB$ and the frequency Ω_1. It is usually difficult to obtain the value of B from the low-frequency amplitude because its value is hidden by low-frequency perturbations. The damping coefficient can be obtained using the maximum-amplitude point if available.

Because of the imperfections of the hinged support and the parasitic stiffness, the values of dissipation and nondamped eigenfrequency, and thus A and B, change from one test to another, although the value of AB remains constant for the same excitation level. This preservation of AB, observed experimentally, can be verified with Eqs. (3) because the product AB does not depend on Ω_0' or γ. The damping test is, to the authors' knowledge, the only accurate procedure to estimate the dissipation and the parameter A, and its results will be extrapolated to other tests. As already mentioned, the determination of A, B, and γ is not essential to the calibration technique because AB is controlled.

Experimental Results for the Pendulum Response

Several damping tests have been carried out on different configurations. The oscillation shows the damped behavior described by the preceding analysis. Two series of data are considered separately, the maxima and the minima, due to zero offset introduced by the imbalance of the pendulum. Each fits satisfactorily a straight line, as described by Eq. (9). From one configuration we obtain the damped period $\Delta = 2.25 \pm 0.01$ s, and from the average of the slopes of the two regression lines, $\gamma = 0.174$ and $\Omega_0' = 1.80$ Hz. For the pendulum under consideration, $L_e = 17.5$ cm; hence, $A = 2.2$ and $\Omega_1 = 1.94$ Hz.

The parameter B, as already mentioned, has to be obtained from direct measurement on the amplitude-responsecurve. Figure 6 shows the results of an oscillation amplitude test. In this case $\theta_\infty = AB = V_{os}/(H_{os}L_{os}) \approx 2.42 \times 10^{-6}$ (at $\omega = 5$ Hz, assumed close to the asymptotic value). For this particular test, the value of

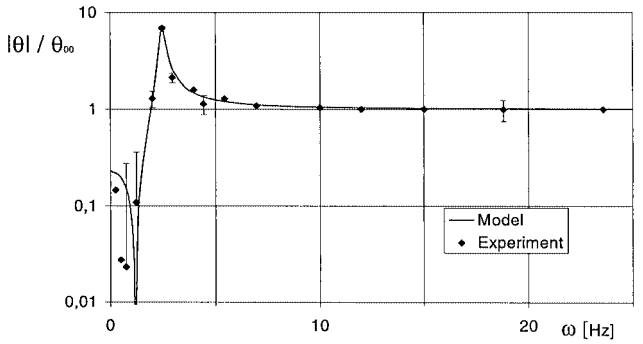

Fig. 7 Matching of the model and an amplitude test: $A = 4.38$, $B = 4.6 \times 10^{-7}$, and $\gamma = 0.056$.

AB corresponds to one quarter of the maximum excitation amplitude, although it is still above the optical resolution limit. Full-scale excitation would give a value close to the design point (Table 1), consistent with the design goals. The parameter B can be obtained in this test from the low-frequency amplitude. Thus, we have $A = 1.72$ and $B = 1.35 \times 10^{-6}$. This shows the variability of the pendulum parameters from test to test due to the different configurations that modify the parasitic stiffness and the damping coefficient. Low-frequency perturbations and noise have an important effect in the measurements, especially at the amplitude zero point x_1. The value of x_1 predicted by the linear model is $\sqrt{(g/L_e)} \approx 1.15$ Hz, whereas 1.475 Hz is indicated in Fig. 6. The difference is indicative of errors in the experimental determination caused by the low-frequency perturbations already mentioned and second-order terms not retained in the model that become relevant when first-order terms cancel out. Furthermore, the acceleration response in Fig. 6 does not show zero-amplitude points because they have been smoothed out. These are the reasons for not using characteristic frequencies for the determination of parameters; only the upper frequency range is useful in this configuration.

In Fig. 7 another amplitude-response test is shown. Although A and B are different, $\theta_\infty = AB \approx 2.0 \times 10^{-6}$, very close to the earlier value for the result in Fig. 6. After matching the nondimensional parameters, the correlation between experimental results and the theoretical model is good. The useful range lies above 3 Hz in this case. The excitation amplitude can be increased for controlling the acceleration level, and the measurement range can be easily changed to enable lower-frequency measurements. The present configuration behaves as a high-pass filter, but using an A lower than unity, the low-frequency range would be enhanced, increasing at the same time the cutoff frequency as required by microgravity applications.[6]

Uncertainty Analysis

In this section a method for the assessment of uncertainties, an essential issue in calibration techniques, is described. It follows the principles stated in the *ISO Guide to the Expression of Uncertainty*.[10] Uncertainties are classified in two categories: type I, which can be objectively deduced from the measurements and statistical procedures, and type II, which is evaluated by scientific judgment based on available information, such as previous data, experience, or general knowledge. As uncertainty is associated to standard deviation, the combined uncertainty for the scale factor measurement is $u^2_{\mathrm{SF}} = u^2_{\mathrm{SF,I}} + u^2_{\mathrm{SF,II}}$.

Introducing in Eq. (1) the expression for the accelerometer's response and using the proportionality of the optical sensor output to the pendulum rotation $|V_{\mathrm{os}}| = H_{\mathrm{os}} L_{\mathrm{os}} |\theta|$, we have

$$\mathrm{SF}(\omega) = \frac{H_{\mathrm{os}} L_{\mathrm{os}}}{\left| g - L_a \omega^2 \right|} \frac{|V_a|}{|V_{\mathrm{os}}|} \tag{10}$$

In view of Eq. (10), sensitivity to errors can be attributed to the determination or measurement of the excitation frequency, the output voltages, the accelerometer rotation radius, and the optical parameters. Axis misalignment and transverse sensitivity of the accelerometer are also responsible for uncertainty. The influence coefficients are calculated from Eq. (10), which corresponds to the ideal situation of perfect alignment and zero transverse sensitivity. Misalignment and transverse sensitivity effects will be considered afterward. Hence, the following influence coefficients $C_i = |\partial \mathrm{SF}/\partial i|$ can be directly calculated:

$$C_\omega = \frac{\mathrm{SF} \cdot 2 L_a \omega}{\left| g - L_a \omega^2 \right|}, \qquad C_a = \frac{\mathrm{SF}}{|V_a|}, \qquad C_{\mathrm{os}} = \frac{\mathrm{SF}}{|V_{\mathrm{os}}|}$$
$$C_{La} = \frac{\mathrm{SF} \cdot \omega^2}{\left| g - L_a \omega^2 \right|}, \qquad C_H = \frac{\mathrm{SF}}{H_{\mathrm{os}}}, \qquad C_{L\mathrm{os}} = \frac{\mathrm{SF}}{L_{\mathrm{os}}} \tag{11}$$

These sensitivity coefficients contribute to the uncertainty through the error propagation law,

$$u^2_{\mathrm{SF}} = \sum C_i^2 u_i^2 \tag{12}$$

Besides the uncertainty introduced by the parameters, the misalignment error introduces an uncertainty in the input acceleration. In Eq. (1), A_θ should be replaced by $A_{\mathrm{axis}} = \boldsymbol{A} \cdot \boldsymbol{e}$, the projection of the net acceleration vector onto the sensitive axis of the accelerometer, whose exact orientation is unknown. Using the results of the accelerometer model, in the pendulum intrinsic reference frame

$$\boldsymbol{A} \approx \left(g - L_a \omega^2\right) \theta \boldsymbol{u}_\theta + \delta_a \omega^2 \theta \boldsymbol{u}_r + 0 \cdot \boldsymbol{u}_r \times \boldsymbol{u}_\theta \tag{13}$$

$$\boldsymbol{e} \approx \boldsymbol{u}_\theta + \delta\alpha \boldsymbol{u}_r + \delta\beta \boldsymbol{u}_r \times \boldsymbol{u}_\theta \tag{14}$$

where $\delta\alpha$ and $\delta\beta$ are the misalignment angles of the accelerometer's sensitive axis to the pendulum frame, which can be considered small. Thus, we have $A_{\mathrm{axis}} \approx A_\theta + \delta\alpha A_r$. Inserting this in Eq. (1) in place of A_θ and retaining the first term of the series expansion for small misalignment angles,

$$\mathrm{SF} \approx |V_a|/|A_\theta| [1 - (|A_r|/|A_\theta|)\delta\alpha] \tag{15}$$

Equation (15) is deterministic, i.e., if the misalignment angle were known, its effect on the scale factor could be calculated.[6] However, inasmuch as misalignments are not measured in this particular application, a stochastic interpretation is more appropriate, and hence, using Eq. (6), the influence coefficient of misalignment can be computed as

$$C_\alpha = \left| \frac{\partial \mathrm{SF}}{\partial \delta\alpha} \right| \approx \frac{\mathrm{SF} \cdot \delta_a \omega^2}{\left| g - L_a \omega^2 \right|} = \delta_a C_{La} \tag{16}$$

Slightly more subtle is the evaluation of transverse sensitivity, which is also faced from a stochastic point of view as an uncertainty for the scale factor. In Eqs. (1) and (15), the accelerometer's output voltage must be considered to be the superposition of two signals, the axial and the transverse contributions, which are approximately tangential and radial, respectively. Hence, $V_a \approx V_{a,\theta} + V_{a,r}$. From the manufacturer's specifications, the transverse contribution can be assessed as $V_{a,r} \approx A_r \lambda\, \mathrm{SF}$, resulting in the following influence coefficient due to transverse sensitivity:

$$C_\lambda \approx \mathrm{SF}(|A_r|/|A_\theta|) = \delta_a C_{La} \tag{17}$$

which is the same as for a misalignment. This is physically correct because transverse sensitivity can be mainly attributed to an internal misalignment. The expression for the relative uncertainty, considering the mentioned contributions, is then

$$\frac{u^2_{\mathrm{SF}}}{\mathrm{SF}^2} = \left(\frac{2 L_a \omega^2}{g - L_a \omega^2} \right)^2 \frac{u^2_\omega}{\omega^2} + \frac{u^2_a}{V_a^2} + \frac{u^2_{\mathrm{os}}}{V^2_{\mathrm{os}}} + \left(\frac{L_a \omega^2}{g - L_a \omega^2} \right)^2 \frac{u^2_{La}}{L_a^2}$$
$$+ \frac{u^2_{L\mathrm{os}}}{L^2_{\mathrm{os}}} + \frac{u^2_H}{H^2_{\mathrm{os}}} + \left(\frac{\delta_a \omega^2}{g - L_a \omega^2} \right)^2 \left(u^2_\alpha + u^2_\lambda \right) \tag{18}$$

Equation (18) demonstrates the high sensitivity to errors when measuring close to the characteristic frequency $\omega = \sqrt{(g/L_a)}$. Moreover, the smaller the centering parameter δ_a and the higher the optical radius and sensitivity, the smaller the uncertainty. Table 2 shows typical type II uncertainty contributions to Eq. (18).

Table 2 Typical type II uncertainties in Eq. (18)

Denomination and remarks	Influence coefficient	Uncertainty	Contribution to $(u_{SF}/SF)^2$
Acceleration resolution $= 1E-4$ V $V_a = 0.0279$ V	1.0	$\frac{u_a}{V_a} = \frac{\text{resolution}}{V_a\sqrt{12}} \approx 1E-3$	$1E-6$
Oscillation resolution $= 1E-5$ V $V_{os} = 0.00107$ V	1.0	$\frac{u_{os}}{V_{os}} = \frac{\text{resolution}}{V_{os}\sqrt{12}} \approx 3E-3$	$9E-6$
Frequency resolution $= 1$ mHz $\omega = 18$ Hz	$\left\lvert\frac{2L_a\omega^2}{g-L_a\omega^2}\right\rvert \approx 2.0$	$\frac{u_\omega}{\omega} = \frac{\text{resolution}}{\omega\sqrt{12}} \approx 2E-5$	$2E-9$
Rotation radius, mm $L_a = 94$, $u_{La} \le 1.5$	$\left\lvert\frac{L_a\omega^2}{g-L_a\omega^2}\right\rvert \approx 1.0$	$\frac{u_{La}}{L_a} \approx 2E-2$	$5E-4$
Optical length, mm $L_{os} = 471$, $u_{Los} \approx 1/\sqrt{12}$	1.0	$\frac{u_{Los}}{L_{os}} \approx 6E-4$	$4E-8$
Optical sensitivity, V/mm $H_{os} \approx 1.02$, $u_H \approx 0.01$	1.0	$\frac{u_H}{H_{os}} \approx 1E-2$	$1E-4$
Misalignment, mm $\delta_a \approx 10$	$\left\lvert\frac{\delta_a\omega^2}{g-L_a\omega^2}\right\rvert \approx 0.1$	$u_\alpha \approx (2E-2)/\sqrt{12}$	$3E-7$
Transverse sensitivity $u_\lambda \approx 0.01$	$\left\lvert\frac{\delta_a\omega^2}{g-L_a\omega^2}\right\rvert \approx 0.1$	$u_\lambda \approx 0.01$	$1E-6$

Table 3 Sensitivity calibration of the ISOSHEAR accelerometer[a]

f, Hz	V_e, V	V_a, mV	V_{os}, mV	A_θ, $10^{-6}\,g_0$	SF, V/g_0	SF, pC/g_0
25.5	1.0	54.2	1.090	556	0.975	1052
18.0	1.0	27.9	1.075	272	1.025	1106
18.0	2.0	59.9	2.310	585	1.024	1105
13.5	1.0	16.1	1.080	153	1.054	1137
13.5	2.0	34.6	2.315	328	1.056	1139
11.0	0.5	5.20	0.510	48	1.088	1173
11.0	1.0	10.9	1.080	100	1.083	1169
11.0	2.0	23.4	2.325	217	1.080	1165

[a]Acceleration gain $= 100$, $L_a = 94 \pm 1.5$ mm, $H_{os} = 1.024 \pm 0.001$ V/mm, $L_{os} = 471 \pm 2$ mm, $u_{SF}/SF = 0.02$.

Accelerometer Calibration Tests

The calibration technique has been applied to the shear piezoelectric accelerometers ENDEVCO ISOSHEAR® 7703a-1000 and ISOTRON® 7751-500. The ISOSHEAR accelerometer has a negative slope of the frequency response in the useful range of frequencies, whereas the ISOTRON, whose signal is internally treated, has an almost constant response, except for the dc decay. The nominal sensitivity of the ISOSHEAR specimen is 1079 pC/g at 100 Hz, and it is 485 mV/g for the ISOTRON. Sensitivity and resolution have been measured at different frequencies, the resolution being determined at the lowest detected acceleration level, while preserving linearity over amplitude.

A record of the outputs during a sensitivity test is shown in Fig. 8. Notice the peaks at 50 Hz, which come from the ac line, and the peak at 2 Hz, the eigenfrequency of the pendulum. The signal information is contained in the 17.5-Hz peak, which is the excitation frequency. In Table 3, several measured sensitivities are listed at different frequencies for the ISOSHEAR accelerometer. At each frequency, the several excitation levels show repeatability within the measurement errors. The associated total uncertainty is dominated by $u_{La}/L_a \approx 0.02$ for type II, whereas type I uncertainty is negligible. Thus, we have for $L_a = 94 \pm 1.5$ mm a total uncertainty $u_{SF}/SF \approx 0.02$, which can be improved if necessary by modifying the hinged support. The frequency response has a negative slope, as expected, and the absolute values of the sensitivity are close to the nominal given by the manufacturer but slightly different and obtained at much lower acceleration levels. Table 4 is the summary of sensitivities measured on the ISOTRON accelerometer. Type I uncertainties in this case are not negligible due to the noisy behavior of the accelerometer. The total uncertainty is in this case $u_{SF}/SF = 0.04$.

Table 4 Sensitivity calibration of the ISOTRON accelerometer[a]

f, Hz	V_e, V	V_a, mV	V_{os}, mV	A_θ, $10^{-6}g_0$	SF, mV/g_0
20.0	1.0	152	1.08	337	451
17.5	1.0	115	1.08	257	447
10.0	1.0	33	1.11	85	388

[a]$L_a = 94 \pm 1.5$ mm, $H_{os} = 1.024 \pm 0.001$ V/mm, $L_{os} = 471 \pm 2$ mm, $u_{SF}/SF = 0.04$.

Table 5 Resolution test on the ISOSHEAR accelerometer[a]

f, Hz	V_e, V	V_a, mV	V_{os}, mV	A_θ, $10^{-6}\,g_0$	SF, pC/$g_0 \times 10^{-3}$
17.5	0.10	0.55	0.100	5.4	1.10
17.5	0.09	0.48	0.080	4.3	1.20
17.5	0.08	0.43	0.075	4.1	1.14
17.5	0.07	0.38	0.070	3.8	1.08
17.5	0.06	0.33	0.060	3.3	1.10

[a]Acceleration gain $= 100$, $L_a = 22 \pm 1.5$ mm, $H_{os} = 1.024 \pm 0.001$ V/mm, $L_{os} = 471 \pm 2$ mm, $u_{SF}/SF = 0.10$.

Table 5 summarizes the resolution tests performed on the ISOSHEAR accelerometer. Significant variations of the measured scale factor are evident while reducing the excitation level, due to an increase in the relative measurement uncertainty of the oscillation output. Although not reported in Table 5, acceleration levels down to $10^{-7}\,g$ have been measured but with an uncertainty greater than $u_{SF}/SF = 0.10$. The associated uncertainty of the scale factor is too high because of poor behavior of the hinged support ($L_a = 22 \pm 1.5$ mm). This has produced an uncertainty of $u_{SF}/SF = 0.10$, which could have been reduced to 0.04 with a better knowledge of L_a. In any case, the lower bound of the technique has not been

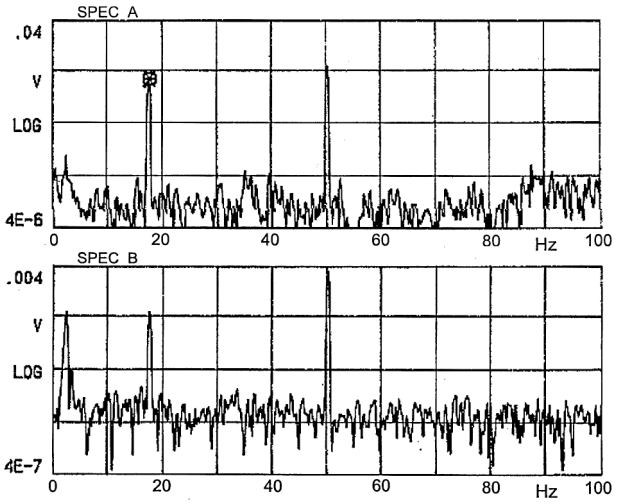

Fig. 8 Frequency spectrum record of a sensitivity test with $L_a = 22$ mm: Channel A is the ISOSHEAR accelerometer and channel B the optical sensor; pointer (⊗) at 17.5 Hz, $V_{os} = 5.11E-4$ V, $V_a = 2.97E-3$ V, frequency resolution $\Delta f = 0.25$ Hz.

reached in this test, and an improvement of the hinged support will reduce the uncertainty. This improvement would consist of minor geometrical changes in the mechanical design.

Conclusions

A calibration device of accelerometers for microvibrations and the corresponding modeling and experimental procedures have been developed. This calibration technique can be applied to accelerometers devoted to microgravity and microvibration applications that range from structural active control to scientific orbiting payloads and spacecraft attitude control. One of the aims has been the exclusive use of an on-Earth laboratory with standard equipment. The specified measurement range is 10^{-7}–10^{-2} g and 0–100 Hz. The analysis and results presented include the models of the calibration device and the design procedure, the tests performed on the calibration device, the analysis and assessment of measurement uncertainty, and the application of the technique to commercial accelerometers for the measurement of the sensitivity and the resolution.

Two commercial accelerometers have been calibrated in the required range of acceleration and frequency. Sensitivity has been measured in the 10^{-6}–10^{-4} -g range with an uncertainty of $u_{SF}/SF \approx 0.02$–0.04. Accelerations down to 10^{-7} g have been measured but with a moderately higher uncertainty.

As deduced from the uncertainty analysis, improvements can be introduced to increase the accuracy. The main difficulties encountered arise from the behavior of the hinged support used. They are the uncertainty in the rotation radius L_a, the main source of uncertainty, and vibration eigenfrequencies, limiting the actual frequency range of measurement. Another difficulty is the parasitic stiffness, which is responsible for changing the pendulum eigenfrequency from test to test, although the characteristic oscillation amplitude θ_∞ remains constant. However, the robustness of the technique has been proven because the accelerometers can be calibrated without knowledge of the exact values of the pendulum parameters A, B, and γ. This is due to the fine excitation control and the precise measurement of the pendulum oscillation amplitude.

Appendix: Model Equations for the Calibration Pendulum

This Appendix is a deduction of the pendulum model, showing the simplifications introduced. Consider Fig. 2 for the definition of the pendulum parameters. The dynamical system is described by Lagrange's equation

$$\frac{\mathrm{d}}{\mathrm{d}t}\left(\frac{\partial L}{\partial \dot{\theta}}\right) - \frac{\partial L}{\partial \theta} = 0$$

which applied to the Lagrangian function L of the system yields the equation of motion

$$\left[I + m\left(L_e^2 + u^2\right)\right]\ddot{\theta} + 2mu\dot{u}\dot{\theta} + mL_e\ddot{u} + (ML_M + mL_e)g\sin\theta + (M\delta_M + mu)g\cos\theta = 0 \qquad \text{(A1)}$$

Small oscillation amplitudes will be considered. The excitation has been imposed as the geometric condition $u = \delta_m + |u|\sin(\omega t)$, from which a Mathieu-type equation is obtained:

$$\left(I + m\left\{L_e^2 + [\delta_m + |u|\sin(\omega t)]^2\right\}\right)\ddot{\theta} + \{2m|u|\omega[\delta_m + |u|\sin(\omega t)]\cos(\omega t)\}\dot{\theta} + (MgL_M + mgL_e)\theta = \left(L_e\omega^2 - g\right)m|u|\sin(\omega t) - (M\delta_M + m\delta_m)g$$

This equation can be simplified for $|u| \ll L_e$. Furthermore, because this dynamic model is free of damping and the harmonic coefficient of $\dot{\theta}$ will be negligible compared to real damping, the coefficient of $\dot{\theta}$ can be replaced by a constant to be determined by testing. A linear second-order excited system results, where the nondamped eigenfrequency is

$$\Omega_0 = \sqrt{\frac{(ML_M + mL_e)g}{I + m\left(L_e^2 + \delta_m^2\right)}} \qquad \text{(A2)}$$

This eigenfrequency will be modified by the nonnegligible parasitic stiffness exerted by the connecting wires. Therefore, Ω_0 has to be replaced by an unknown Ω_0' to be determined by testing. Actually, the parasitic stiffness can be modeled with a fictitious spring introducing the eigenfrequency Ω_p and, hence, $\Omega_0'^2 = \Omega_p^2 + \Omega_0^2$.

The term $M\delta_M + m\delta_m$ comes from a balancing error because the center of mass of the system, located in pendulum axes at $[(ML_M + mL_e)\boldsymbol{u}_r + (M\delta_M + m\delta_m)\boldsymbol{u}_\theta]/(M + m)$, has its initial equilibrium position in the local vertical of the hinge point, thus introducing an initial balance error angle of the magnitude $\varepsilon = -(M\delta_M + m\delta_m)/(ML_M + mL_e)$, assumed to be small. This balance error ε appears in the time response as a constant displacement but has no relevance if amplitudes are measured. Finally, after all of these considerations, the following equation is used for modeling:

$$\ddot{\theta} + 2\gamma\Omega_0'\dot{\theta} + \Omega_0'^2\theta = \frac{\left(L_e\omega^2 - g\right)}{I + m\left(L_e^2 + \delta_m^2\right)}m|u|\sin(\omega t) + \Omega_0'^2\varepsilon \qquad \text{(A3)}$$

Removing the initial transient, the amplitude is given by Eq. (2) in nondimensional form, as a function of the dimensionless excitation frequency. The effect of slight damping does not change this amplitude response significantly, but qualitatively there are physical considerations of relevance. The coefficients A and B do not depend on γ, but the frequency of maximum amplitude, obtained by differentiating the amplitude response, changes with the damping as

$$\frac{\Omega_1^2}{\Omega_0'^2} = \frac{1 - A - 2\gamma^2}{1 - A + 2A\gamma^2} \qquad \text{(A4)}$$

Depending on whether $A > 1$ or $A < 1$, damped eigenfrequency Ω_1 will increase or decrease compared to the nondamped eigenfrequency, respectively.

Acknowledgments

This study has been supported by the Spanish Comision Interministerial de Ciencia y Tecnologia, Project ESP 95-0021, and the first author has worked under a grant of the Direccion General de Investigacion Cientifica y Tecnologica. This paper resulted from the cooperation between the Instituto Universitario "Ignacio Da Riva," Universidad Politécnica de Madrid, and the Construcciones Aeronáuticas S.A. (CASA) Space Division, Department of Integration and Testing. The authors wish to thank CASA's authorities and personnel for their support, as well as Carlos Ramos and Nikolai Bezdenejnykh.

References

[1]Glaese, R. M., and Miller, D. W., "Derivation of Zero-Gravity Structural Control Models from Analysis and Ground Experimentation," *Journal of Guidance, Control, and Dynamics*, Vol. 19, No. 4, 1996, pp. 787–793.

[2]Perales, J. M., Meseguer, J., and Martínez, I., "Minimum Volume of Axisymmetric Liquid Bridges Between Unequal Disks in an Axial Microgravity Field," *Journal of Crystal Growth*, Vol. 110, 1991, pp. 855–861.

[3]Monti, R., and Savino, R., "Microgravity Experiment Acceleration Tolerability on Space Orbiting Laboratories," *Journal of Spacecraft and Rockets*, Vol. 33, No. 5, 1996, pp. 707–716.

[4]Meseguer, J., and Perales, J. M., "A Linear Analysis of g-Jitter Effects on Viscous Cylindrical Liquid Bridges," *Physics of Fluids A*, Vol. 3, No. 10, 1991, pp. 2332–2336.

[5]Blanchard, R. C., Larman, K., and Moats, C., "Flight Calibration Assessment of HIRAP Accelerometer Data," AIAA Paper 93-0836, Jan. 1993.

[6]Santiago-Prowald, J., Sanz-Andrés, A., and Bezdenejnykh, N., "On-Earth Calibration of Accelerometers for Microgravity Applications," *Microgravity Science and Technology*, Vol. 9, No. 1, 1996, pp. 46–54.

[7]*Microgravity News*, Vol. 3, No. 4, 1996, pp. 7, 8.

[8]Marchante, E. M., and Muñoz, L., "ARTEMIS Satellite Microvibrations Testing and Analysis Activities," 48th International Astronautics Conf., International Astronautical Federation, Turin, Italy, Oct. 1997.

[9]Blevins, R., *Formulas for Natural Frequency and Mode Shape*, Van Nonstrand Reinhold, New York, 1979, pp. 101–113.

[10]*ISO Guide to the Expression of Uncertainty*, 1st ed., International Organization for Standardization, 1995, pp. 2–22.

R. G. Wilmoth
Associate Editor